Electronic Supporting Information (ESI) for

Modular *O*- vs *N*-coordination of Pyridylidene Amide Ligands to Iron Determines Activity in Alcohol Oxidation Catalysis

Dide G. A. Verhoeven and Martin Albrecht

Departement für Chemie und Biochemie, Universität Bern, Freiestrasse 3, CH-3012 Bern, Switzerland, martin.albrecht@dcb.unibe.ch.

1. NMR spectra

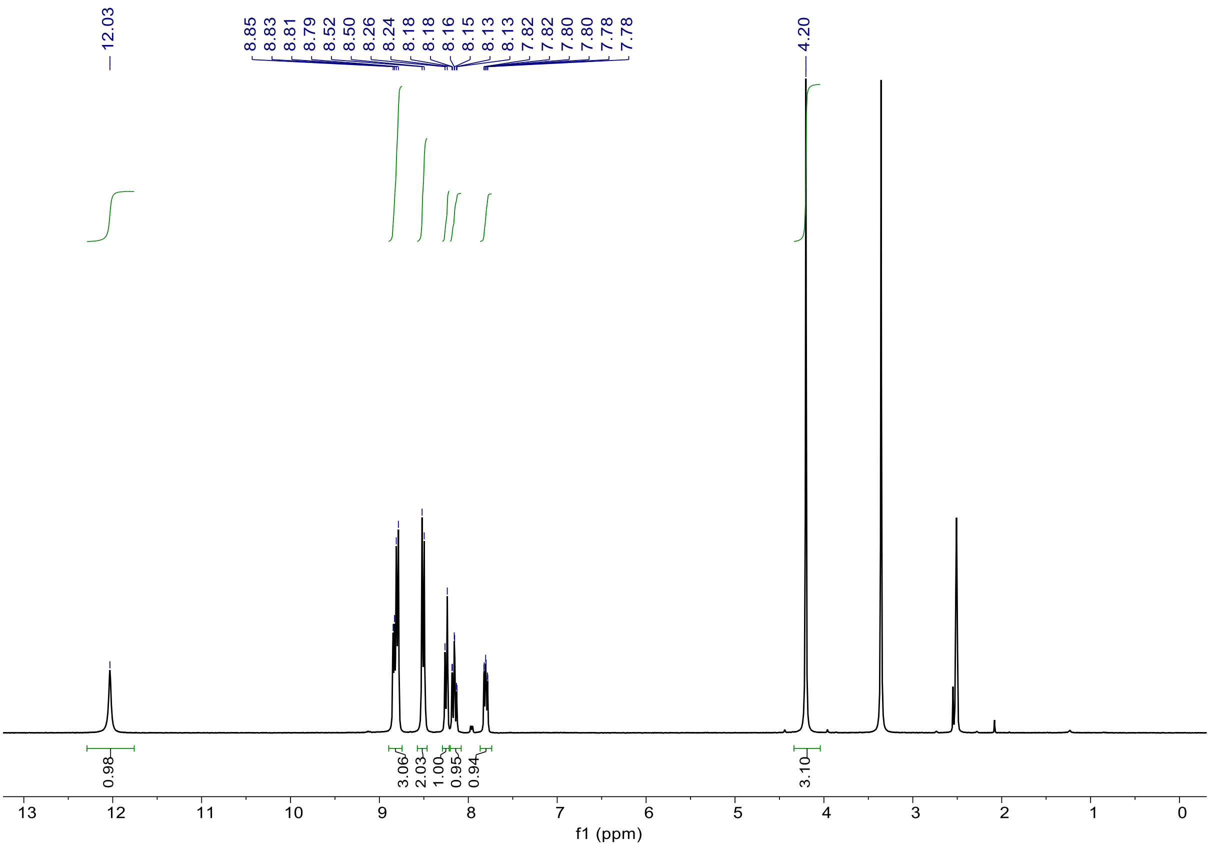

Figure S1. ^{1}H NMR spectrum (300 MHz, DMSO-d_6) of **1**$^{\mathbf{PF_6}}$.

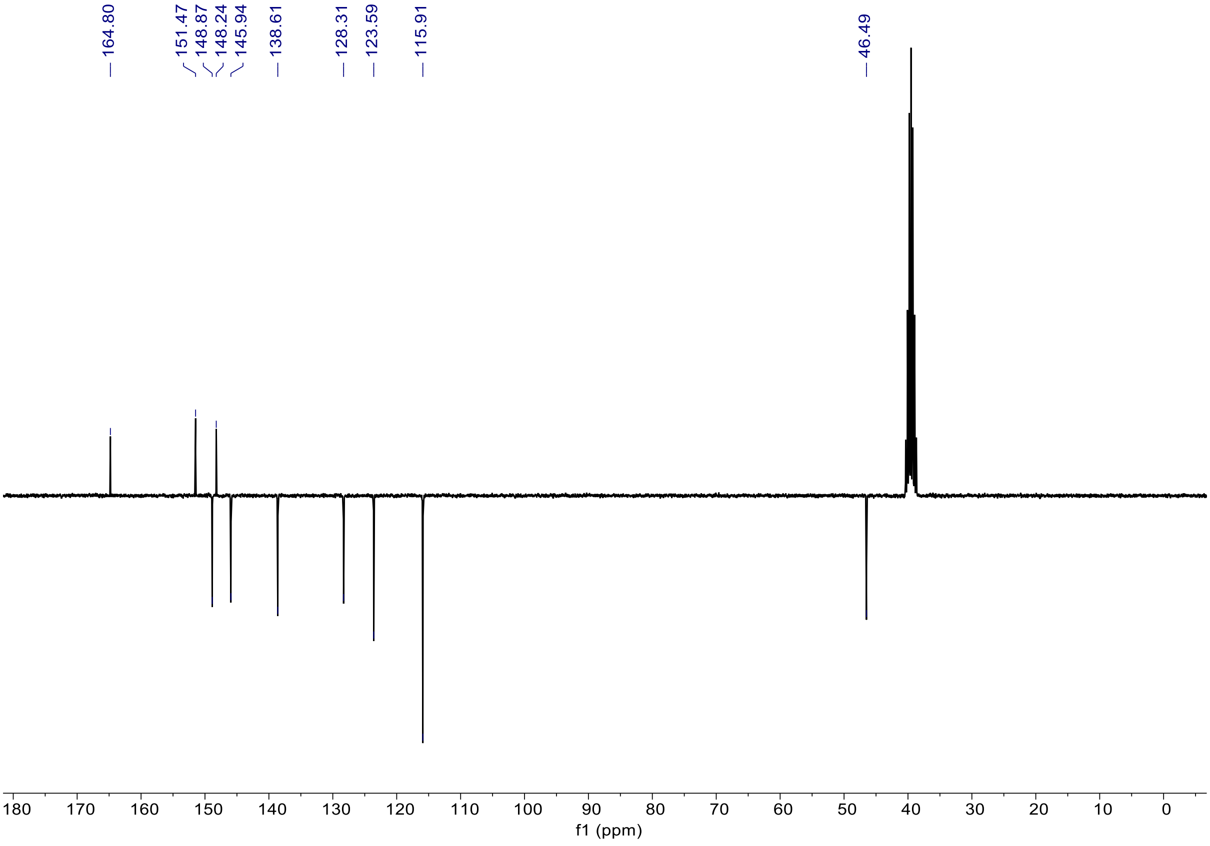

Figure S2. APT ^{13}C NMR spectrum (75 MHz, DMSO-d_6) of **1**$^{\mathbf{PF_6}}$.

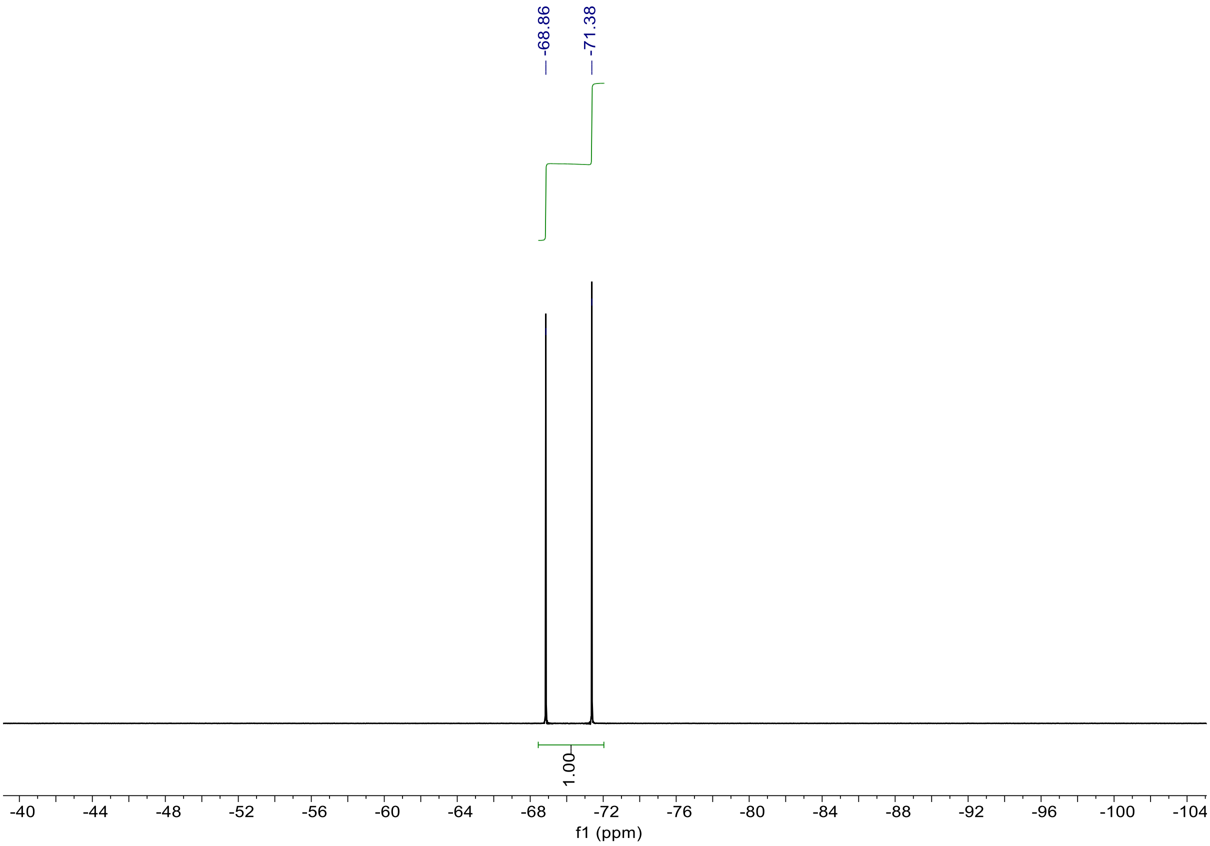

Figure S3. ^{19}F NMR spectrum (282 MHz, DMSO-*d*$_6$) of $\mathbf{1}^{\mathbf{PF_6}}$.

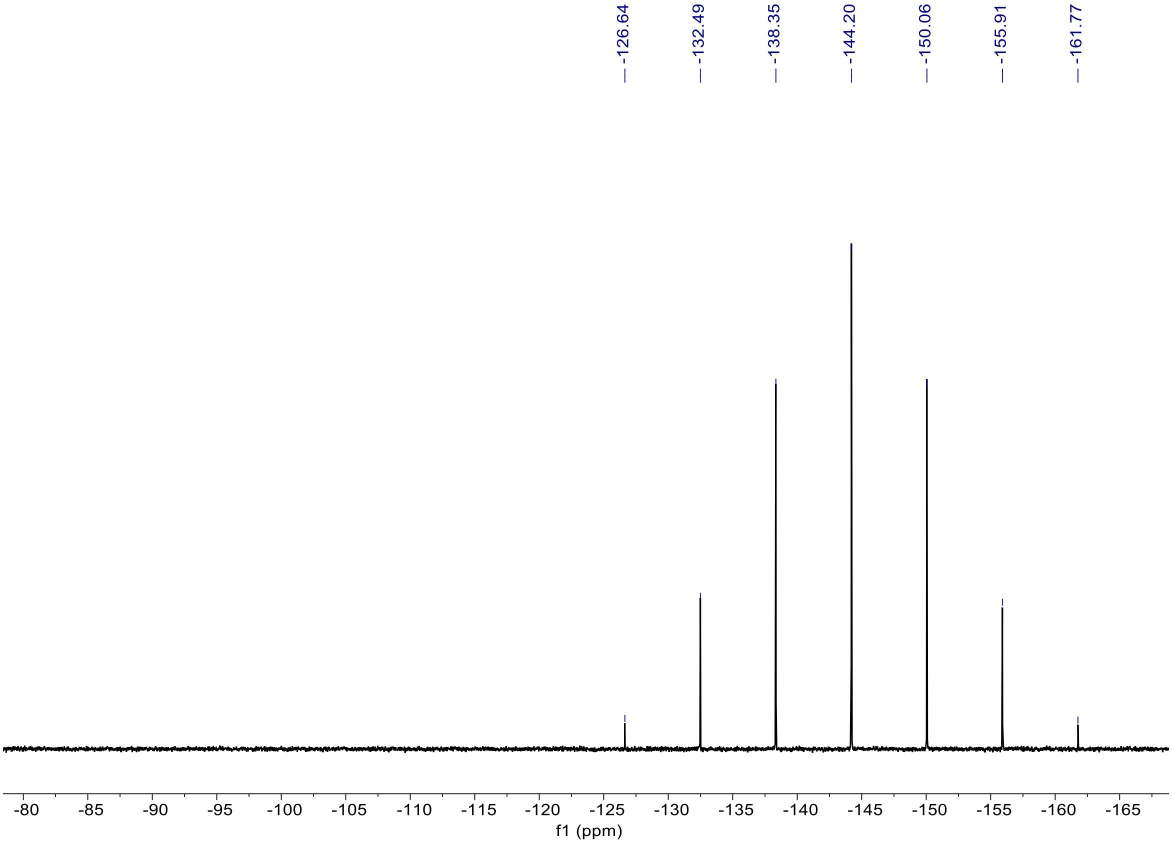

Figure S4. ^{31}P NMR spectrum (121 MHz, DMSO-*d*$_6$) of $\mathbf{1}^{\mathbf{PF_6}}$.

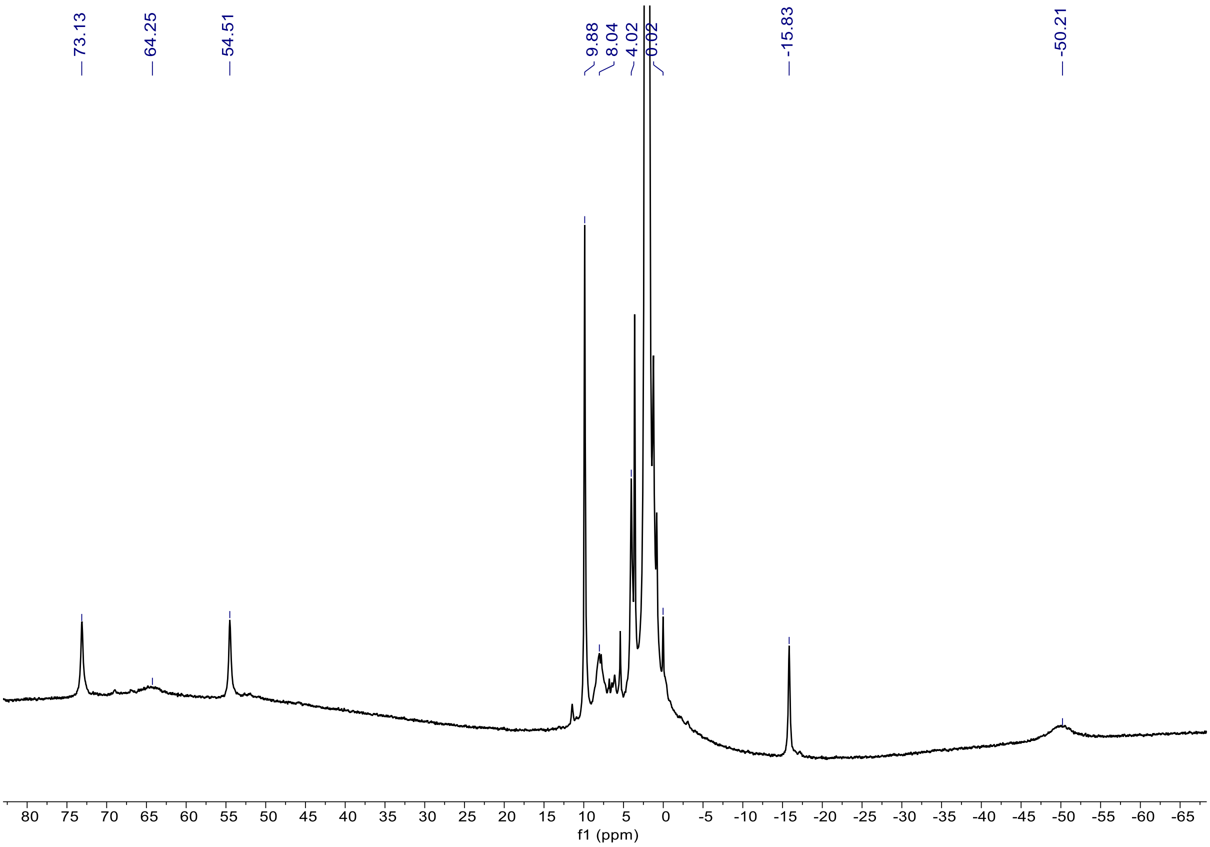

Figure S5. ^{1}H NMR spectrum (300 MHz, CD_3CN) of $[Fe(pyPYA)Cl_2]_2$ (**2**). Relaxation delay and acquisition time at 0.1 second.

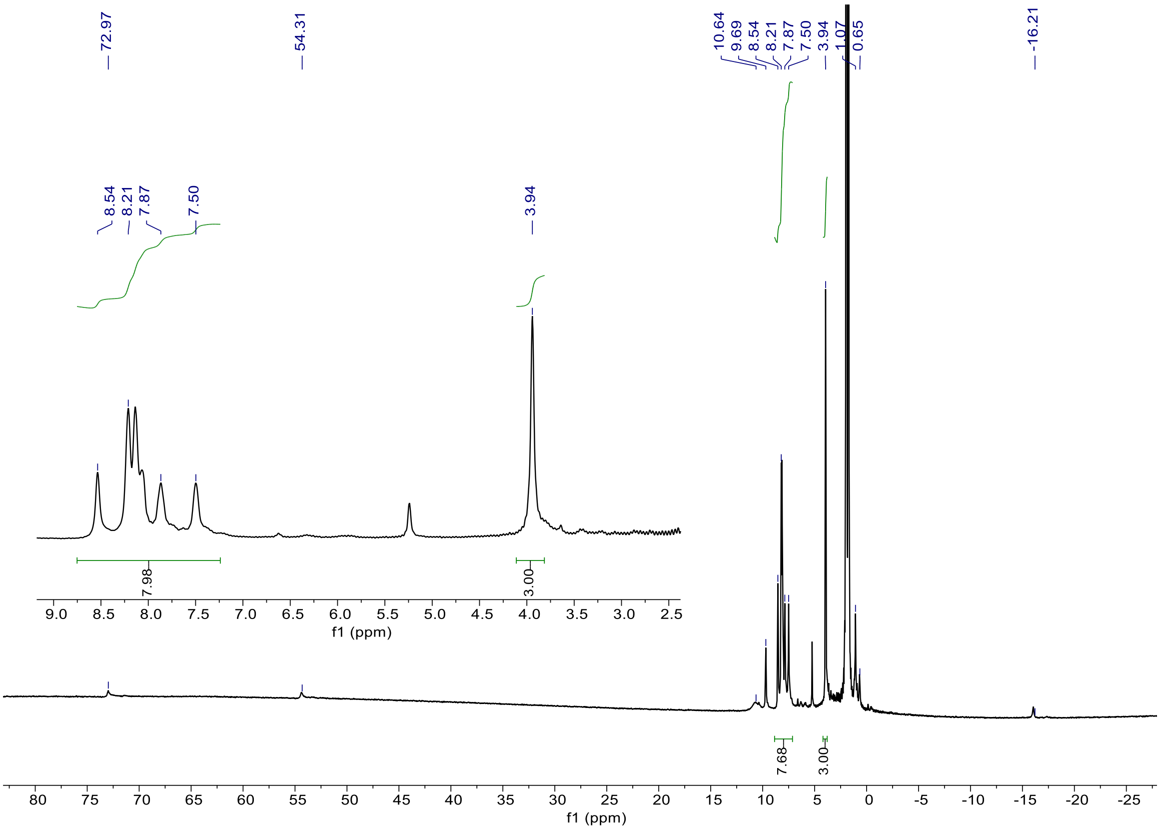

Figure S6. ^{1}H NMR spectrum (300 MHz, CD_3CN) of $[Fe(pyPYA)Cl_2]_2$ (**2**) after one week exposure to air as a solid. Relaxation delay and acquisition time at 0.1 second.

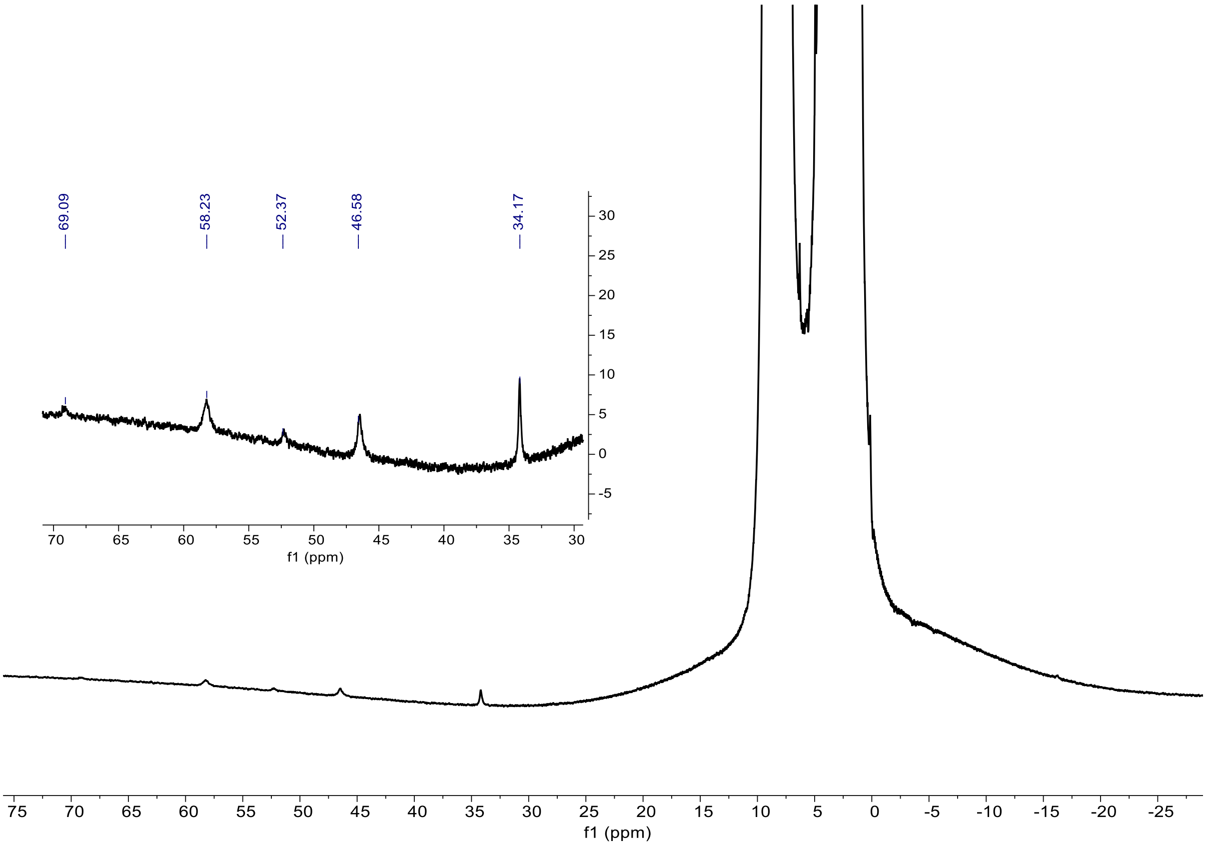

Figure S7. ^{1}H NMR spectrum (300 MHz) of the reaction mixture in the synthesis of [Fe(pyPYA)Cl(py)$_3$]I (**3**). Measurement done without addition of a deuterated solvent (large signals originate from THF and pyridine). Inset: zoom of the paramagnetic signals. Relaxation delay and acquisition time at 0.1 second.

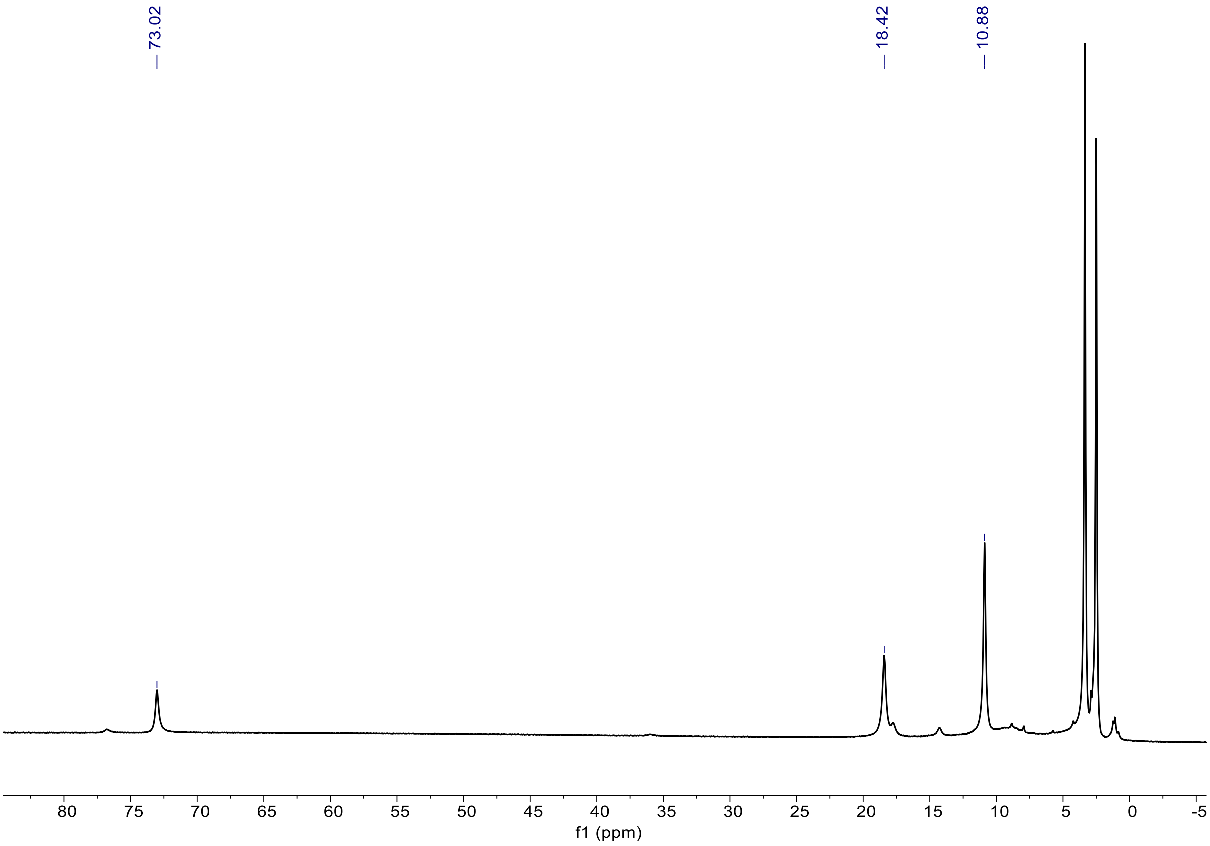

Figure S8. ^{1}H NMR spectrum (300 MHz, DMSO-d_6) of [Fe(pyPYA$_2$)Cl$_2$] (**6**). Relaxation delay and acquisition time at 0.1 second.

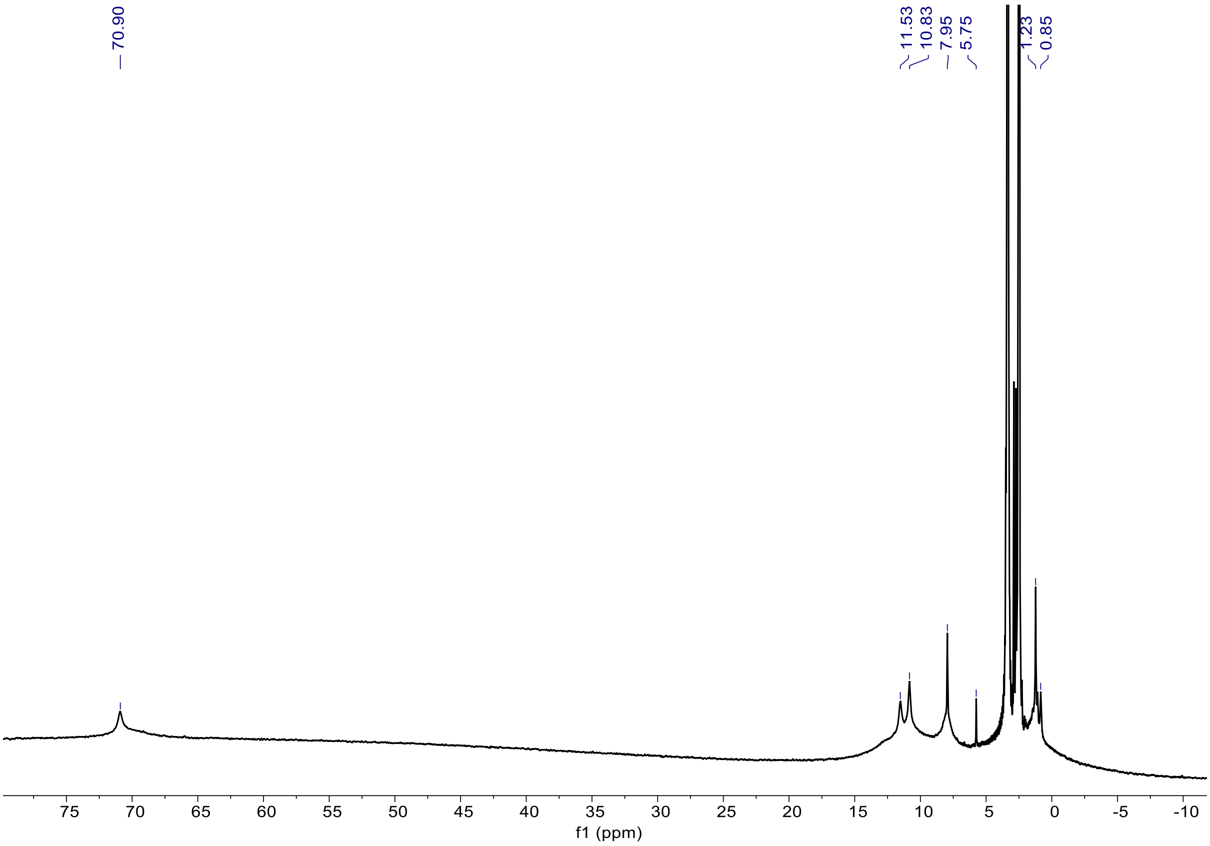

Figure S9. ^{1}H NMR spectrum (300 MHz, DMSO-d_6) of [Fe(pyPYA$_2$)$_2$](PF$_6$)$_2$ (**7**). Relaxation delay and acquisition time at 0.1 second.

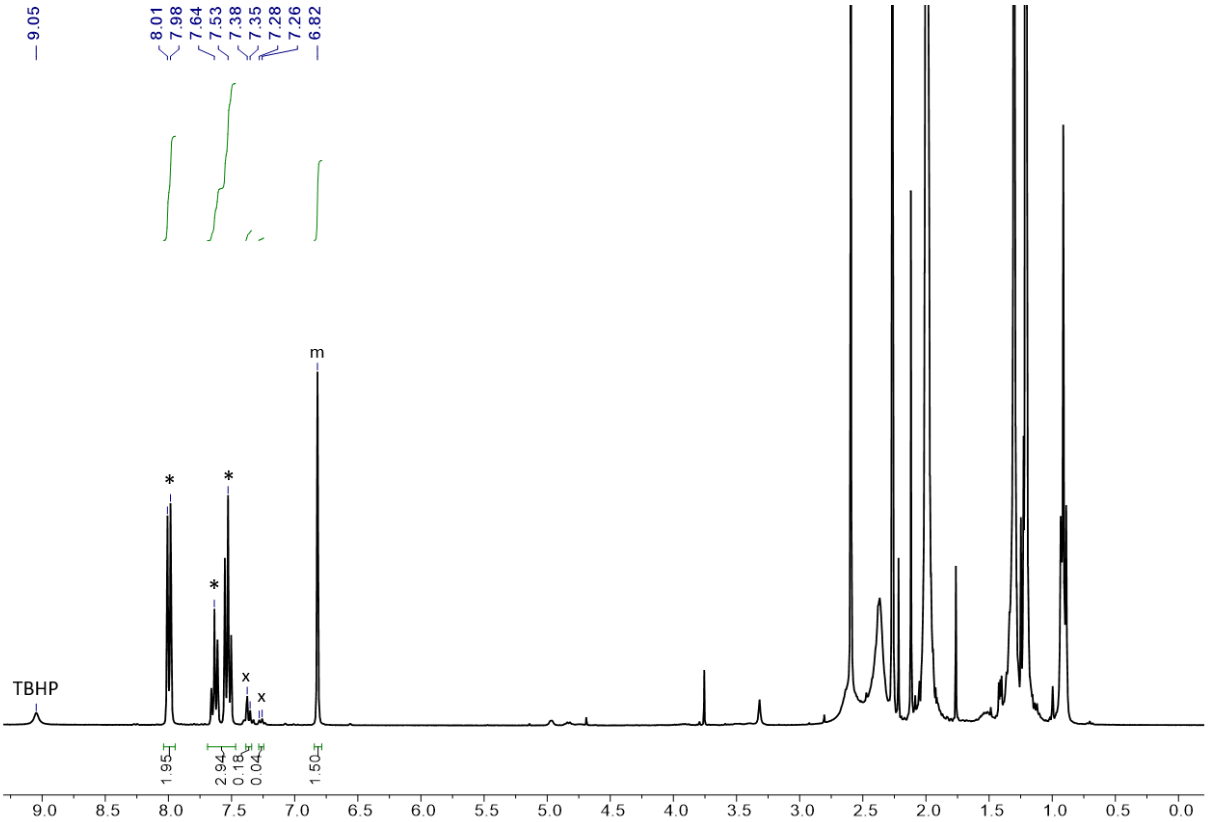

Figure S10. ^{1}H NMR spectrum (300 MHz, CD$_3$CN/CH$_3$CN) of from the catalytic oxidation of 1-phenylethanol to acetophenone with mesitylene as internal standard (resonances labeled with * due to acetophenone, labeled with x due to 1-phenylethanol, and m for mesitylene). Unspecified signals arise from solvents and reaction products.

2. IR spectra

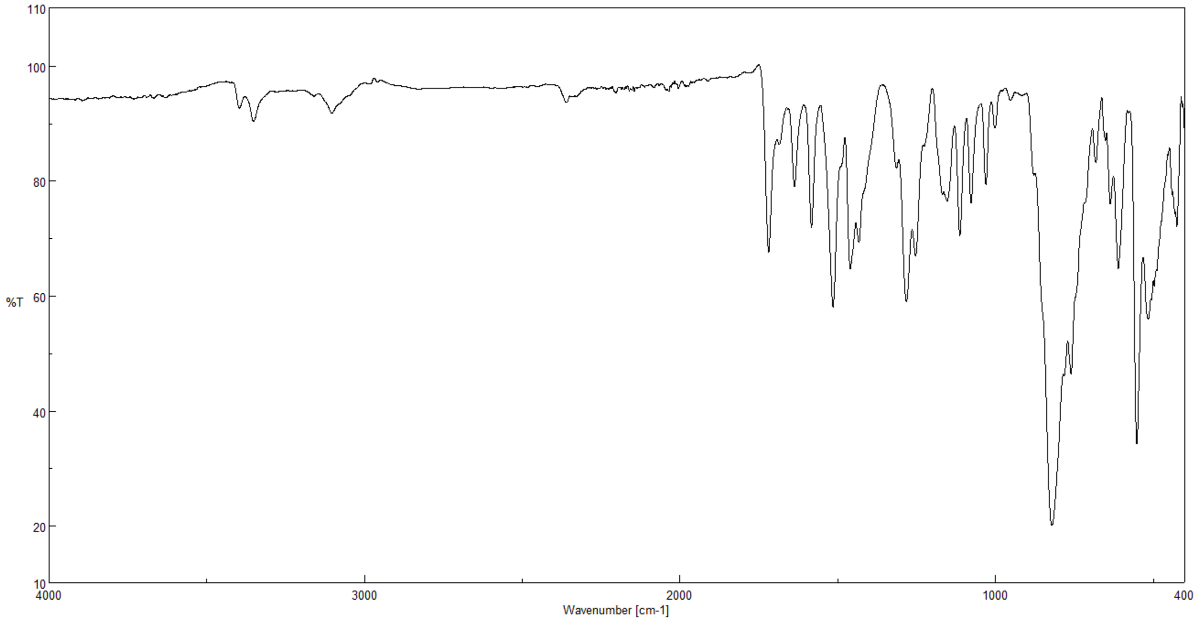

Figure S11. IR spectrum of 1^{PF_6}.

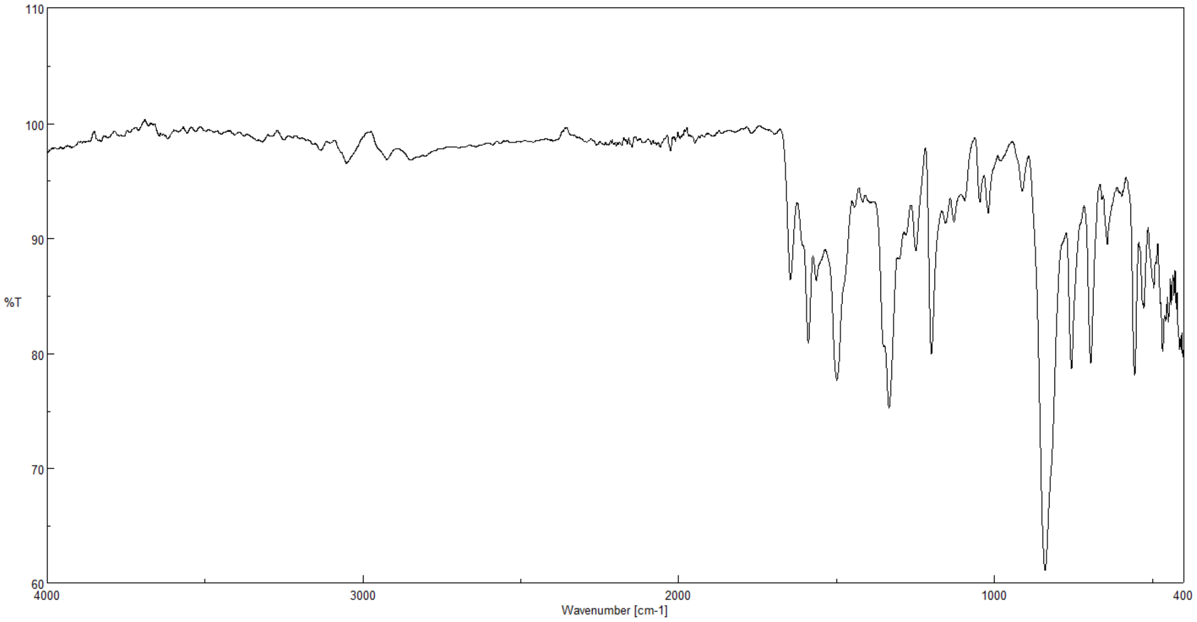

Figure S12. IR spectrum of $[Fe(pyPYA)Cl_2]_2$ (**2**).

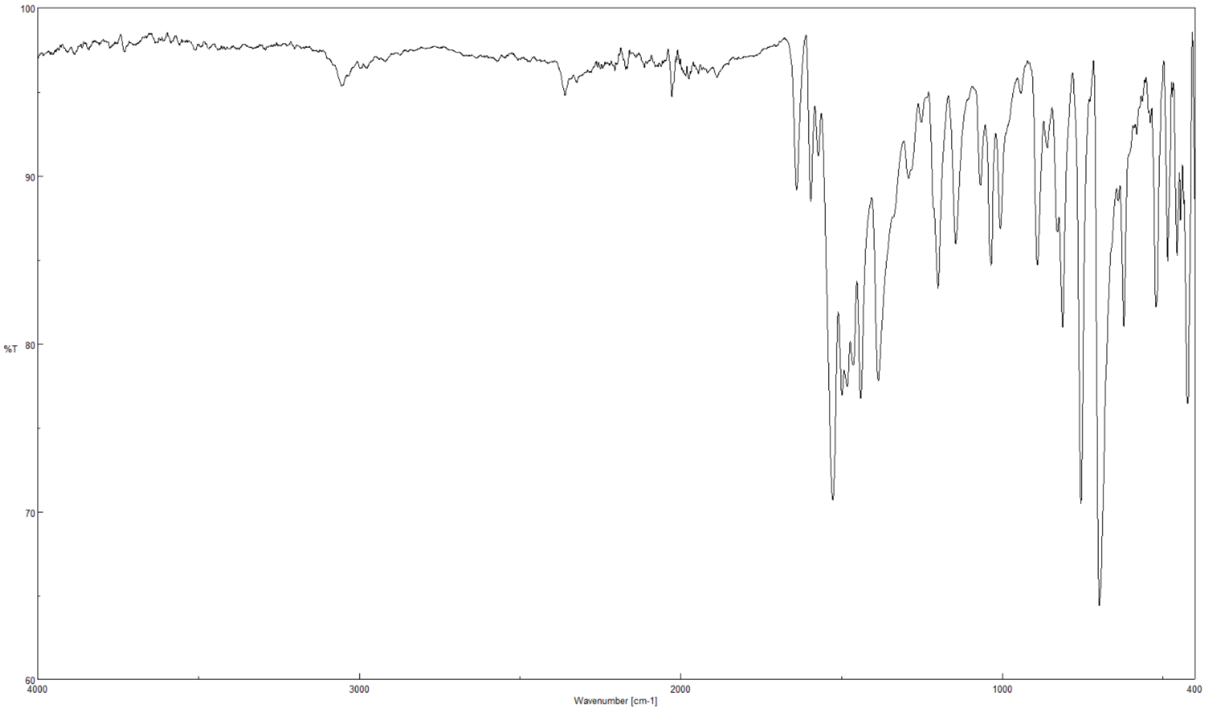

Figure S13. IR spectrum of [Fe(pyPYA)Cl(Py)$_3$]I (**3**).

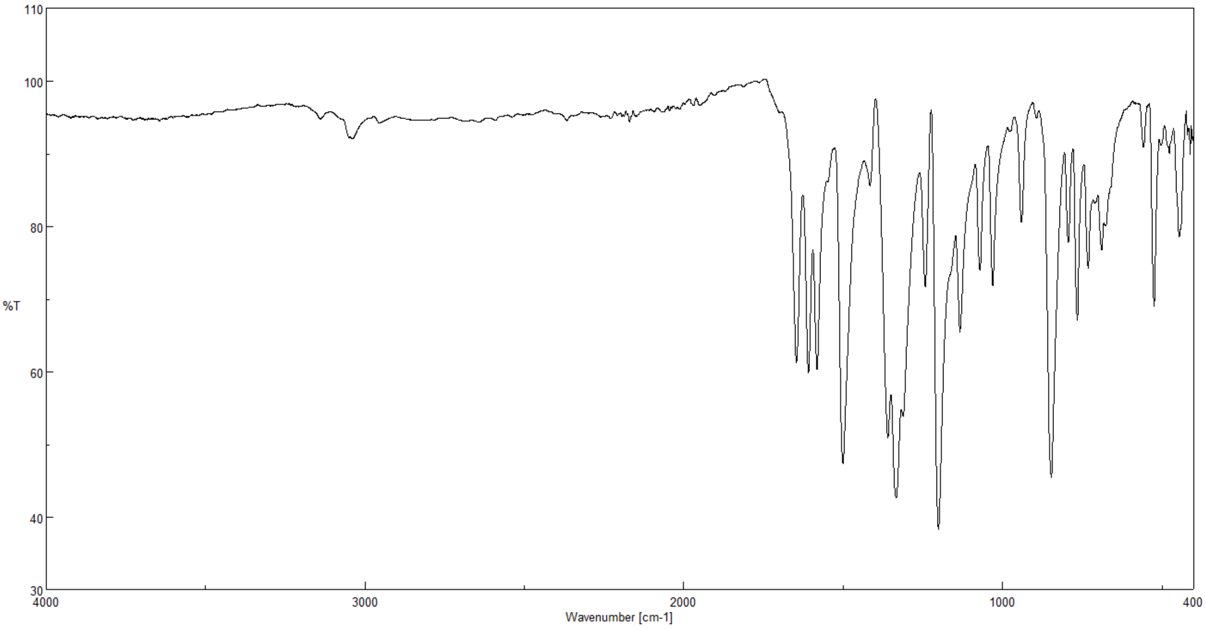

Figure S14. IR spectrum of [Fe(pyPYA$_2$)Cl$_2$] (**6**).

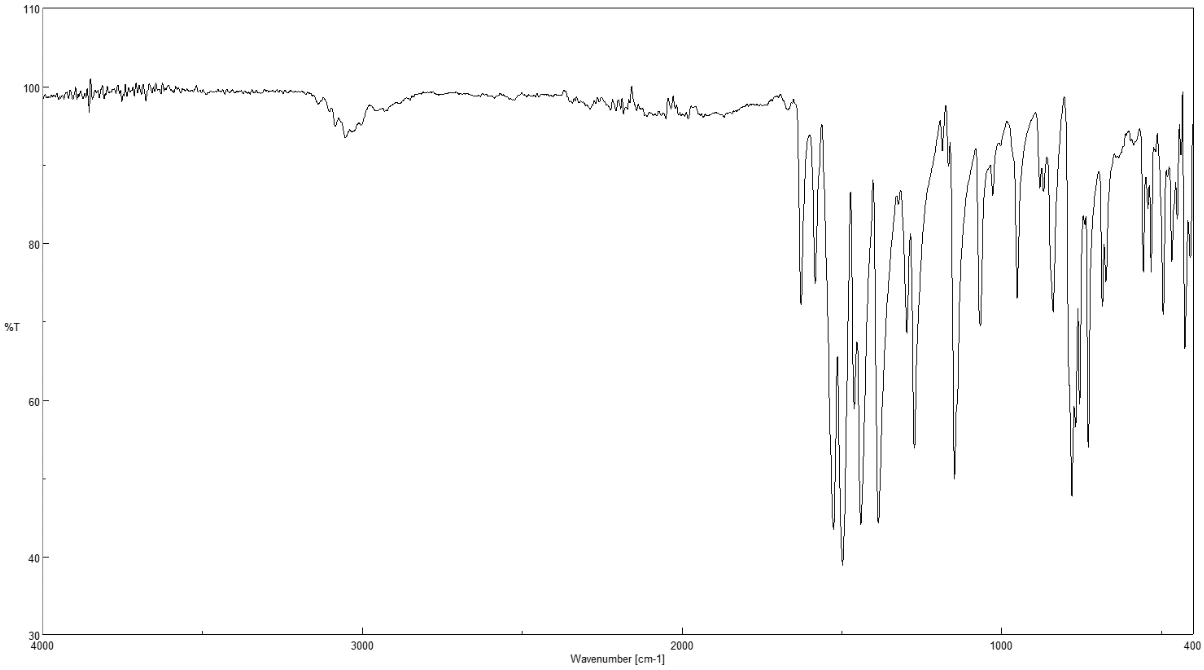

Figure S15. IR spectrum of $[Fe(pyPYA_2)_2](PF_6)_2$ (**7**).

3. Cyclic voltammograms

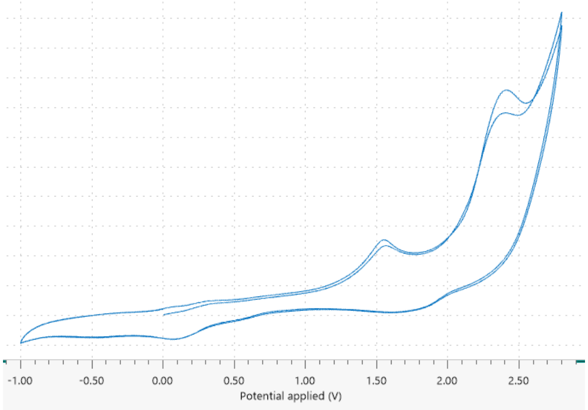

Figure S16. Cyclic voltammogram of **2** in MeCN (*vs* SCE) at 0.25 V sec^{-1}, 3 scans, and NBu_4PF_6 as electrolyte.

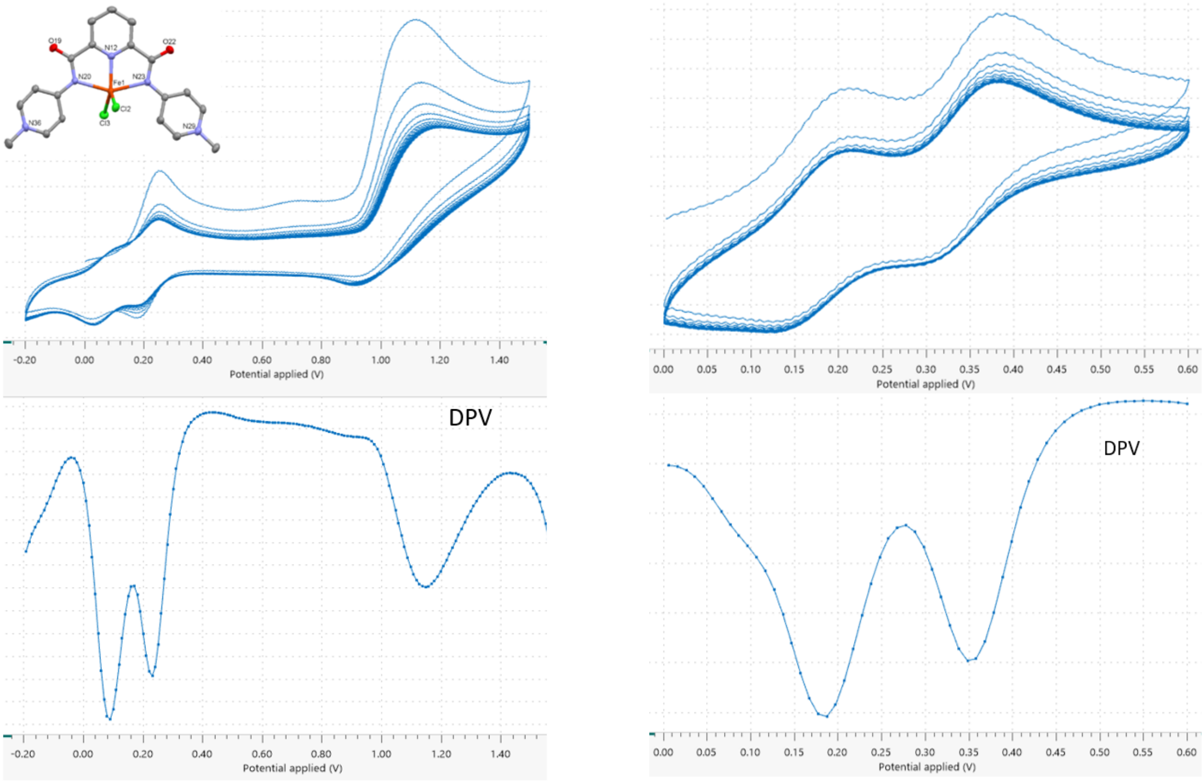

Figure S17. Cyclic voltammogram and DPV (*vs* SCE) of Fe complexes at 0.5 V sec^{-1}, 20 scans, and NBu_4PF_6 as electrolyte. Left: $[Fe(pyPYA_2)Cl_2]$ (**6**) in (anhydrous) DMF. Right: $[Fe(pyPYA_2)_2](PF_6)_2$ (**7**) in MeCN.

Table S1. Cyclic voltammetry values.[a]

Entry	Compound	Solvent	E	*vs* SCE (V)	*vs* Fc$^+$/Fc (V)
1	**2**	MeCN	E_{pa}	1.56	1.16
			E_{pa}	2.41	2.01
2	**6**	DMF	$E_{½}$	0.06	–0.46
			$E_{½}$	0.21	–0.31
			E_{pa}	1.16[b]	0.64[b]
3	**7**	MeCN	$E_{½}$	0.17	–0.25
			$E_{½}$	0.37	–0.05

[a] Measurements were performed with the reference electrode (*vs* SCE). Afterwards, 1 equivalent of ferrocene was added to the mixture and the measurement was performed again to calibrate the values *vs* Fc+/Fc. [b] This weakly reversible signal was attributed to oxidation of water from the solvent.

4. Catalysis

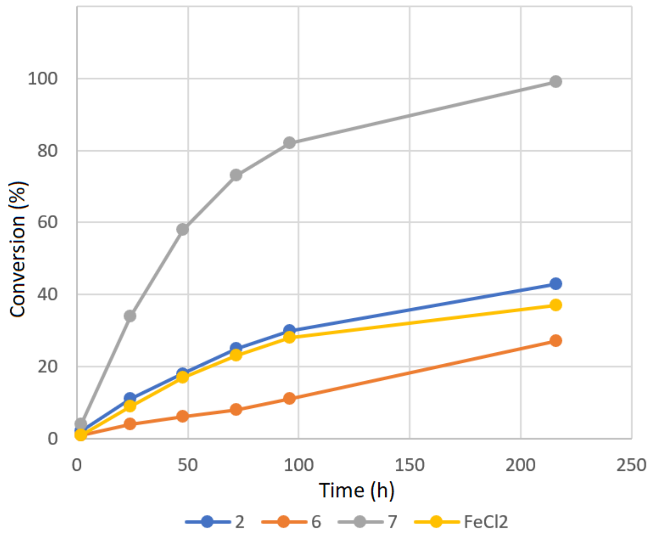

Figure S18. Time-conversion profile of the oxidation of 1-phenylethanol to acetophenone with 0.1 mol% catalyst loading at 25 °C (Table 1, entry 5-8).

Table S2. Comparison between catalyzed and blank oxidations.[a]

Entry	Cat	Substrate	Product	Conversion (time)	
S1 [b]	**7**	Phenyl ethanol	Acetophenone	98 (1 h)	
S2	none	Phenyl ethanol	Acetophenone	<5 (1 h)	90 (24 h)
S3	$\mathbf{1}^{PF_6}$	Phenyl ethanol	Acetophenone	3 (1 h)	11 (24 h)
S4	$\mathbf{4}^{PF_6}$	Phenyl ethanol	Acetophenone	2 (1 h)	19 (24 h)
S5	$\mathbf{5}^{PF_6}$	Phenyl ethanol	Acetophenone	1 (1 h)	6 (24 h)
S6 [c]	$\mathbf{5}^{PF_6}$ + $FeCl_2$	Phenyl ethanol	Acetophenone	36 (1 h)	86 (24 h)
S7	$FeCl_2$	Phenyl ethanol	Acetophenone	50 (1 h)	92 (24 h)
S8 [d]	$FeCl_2$	Phenyl ethanol	Acetophenone	34 (1 h)	89 (24 h)
S9 [b]	**7**	Cyclohexanol	Cyclohexanone	73 (5 h)	75 (24 h)
S10	none	Cyclohexanol	Cyclohexanone	30 (5 h)	58 (24 h)
S11 [b]	**7**	4-phenyl-2-butanol	4-phenyl-2-butanone	51 (5 h)	53 (24 h)
S12	none	4-phenyl-2-butanol	4-phenyl-2-butanone	20 (5 h)	33 (24 h)
S13 [b]	**7**	Thioanisole	Methyl phenyl sulfoxide	57 (2 h)	72 (20 h)
S14	none	Thioanisole	Methyl phenyl sulfoxide	<1 (2 h)	17 (20 h)

[a] General conditions: catalyst (5-7 µmol, 1 mol%), MeCN (0.5 mL), substrate (100 eq), TBHP (2 x 100 eq, 5 M in decane) at the onset and t = 30 min, 80 °C, Ar atmosphere, yields determined by ^{1}H NMR spectroscopy. [b] [Fe] catalyst at 0.5 mol%. [c] 1 mol% of each $FeCl_2$ and $\mathbf{5}^{PF_6}$ were used; conversion reached 58% after 2 h. [d] Reaction performed at 50 °C.

5. X-ray crystal structure data

General description

A crystal was mounted in air at ambient conditions. All measurements were made on an *Oxford Diffraction SuperNova* area-detector diffractometer[S1]] using mirror optics monochromated Mo *K*α radiation (λ = 0.71073 Å) and Al filtered[S2] (complexes **2** and **3**) or on a *RIGAKU Synergy S* area-detector diffractometer[S1] using mirror optics monochromated Cu *K*α radiation (λ = 1.54184 Å) (complexes **6** and **7**).[S2] Data reduction was performed using the *CrysAlisPro*[S1] program. The intensities were corrected for Lorentz and polarization effects, and a numerical absorption correction based on gaussian integration over a multifaceted crystal model was applied. Data collection and refinement parameters are given for all complexes (Table S2-S7). The structure was solved by direct methods using *SHELXT*,[S3] which revealed the positions of the non-hydrogen atoms of the title compound. All non-hydrogen atoms were refined anisotropically. All H-atoms were placed in geometrically calculated positions and refined using a riding model where each H-atom was assigned a fixed isotropic displacement parameter with a value equal to 1.2 Ueq of its parent atom (1.5 Ueq for methyl group). Refinement of the structure was carried out on F^2 using full-matrix least-squares procedures, which minimized the function $\Sigma w(F_o{}^2 - F_c{}^2)^2$. The weighting scheme was based on counting statistics and included a factor to downweight the intense reflections. All calculations were performed using the *SHELXL-2014/7*[S4] program in OLEX2.[S5] Crystallographic data of the complexes reported in this paper have been deposited with the Cambridge Crystallographic Data Centre (CCDC) as supplementary publication numbers 2001555 (**2**), 2001556 (**3**), 2001557 (**6**), 2001558 (**7**).

[Fe(pyPYA)Cl$_2$]$_2$ (2): The unit cell constants and an orientation matrix for data collection were obtained from a least-squares refinement of the setting angles of reflections in the range 1.9° < θ < 27.7°. A total of 1392 frames were collected using ω scans, with 4+4 seconds exposure time, a rotation angle of 1.0° per frame, a crystal-detector distance of 65.0 mm, at T = 173(2) K.

[Fe(pyPYA)Cl(Py)$_3$]I (3): The unit cell constants and an orientation matrix for data collection were obtained from a least-squares refinement of the setting angles of reflections in the range 1.6° < θ < 27.4°. A total of 723 frames were collected using ω scans, with 18+18 seconds exposure time, a rotation angle of 1.0° per frame, a crystal-detector distance of 65.0 mm, at T = 173(2) K.

[Fe(κ^{NNN}-pyPYA$_2$)Cl$_2$] (6): The unit cell constants and an orientation matrix for data collection were obtained from a least-squares refinement of the setting angles of reflections in the range 3.81° < θ < 77.175°. A total of 2400 frames were collected using ω scans, with 3.05 second exposure time (12 seconds for high-angle reflections), a rotation angle of 0.5° per frame, a crystal-detector distance of 65.0 mm, at T = 173(2) K. The intensities were corrected for Lorentz and polarization effects, and an absorption correction based on the multi-scan method using SCALE3 ABSPACK in *CrysAlisPro*[S1] was applied.

[Fe(κ^{ONO}-pyPYA$_2$)Cl$_2$] (8): The unit cell constants and an orientation matrix for data collection were obtained from a least-squares refinement of the setting angles of reflections in the range 4.0° < θ < 76.8°. A total of 3196 frames were collected using ω scans, with 0.25 and 1.0 seconds exposure time, a rotation angle of 0.5° per frame, a crystal-detector distance of 34.0 mm, at T = 173(2) K.

Table S3. Crystal data and structure refinement for complexes **2**, **3**, **6**, and **8**.

	[Fe(pyPYA)Cl$_2$]$_2$ (**2**)	[Fe(pyPYA)Cl(Py)$_3$]I (**3**)
CCDC No	2001555	2001556
Empirical formula	$C_{24}H_{22}Cl_4Fe_2N_6O_2$	$C_{27}H_{26}ClFeIN_6O$
Formula weight	679.97	668.74
Temperature/K	173.00(10)	173.01(10)
Crystal system	triclinic	monoclinic
Space group	P-1	P2$_1$/c
a/Å	7.4259(3)	19.64797(16)
b/Å	8.5641(3)	15.77189(15)
c/Å	10.8957(4)	9.27194(8)
α/°	82.941(3)	90
β/°	84.961(3)	97.2461(8)
γ/°	77.506(3)	90
Volume/Å^3	670.04(4)	2850.29(4)
Z	1	4
ρ_{calc}g/cm^3	1.685	1.558
μ/mm^{-1}	1.517	1.737
F(000)	344.0	1336.0
Crystal size/mm^3	0.358 × 0.221 × 0.046	0.249 × 0.216 × 0.043
Radiation	MoKα (λ = 0.71073)	MoKα (λ = 0.71073)
2Θ range for data collection/°	3.774 to 56.238	3.322 to 56.312
Index ranges	$-9 \le h \le 9$, $-11 \le k \le 11$, $-14 \le l \le 14$	$-25 \le h \le 25$, $-19 \le k \le 20$, $-11 \le l \le 11$
Reflections collected	14261	30955
Independent reflections	3046 [R_{int}= 0.0354, R_{sigma}= 0.0271]	6497 [R_{int}= 0.0314, R_{sigma}= 0.0252]
Data/restraints/parameters	3046/0/173	6497/0/335
Goodness-of-fit on F^2	1.039	1.044
Final R indexes [I>=2σ (I)]	R_1 = 0.0269, wR_2 = 0.0627	R_1 = 0.0315, wR_2 = 0.0743
Final R indexes [all data]	R_1 = 0.0330, wR_2 = 0.0666	R_1 = 0.0409, wR_2 = 0.0791
Largest diff. peak/hole / e Å^{-3}	0.43/-0.30	0.93/-0.33

Table S3 continued. Crystal data and structure refinement for complexes **2**, **3**, **6**, and **8**.

	[Fe(κ^{NNN}-pyPYA$_2$)Cl$_2$] (**6**)	[Fe(κ^{ONO}-pyPYA$_2$)Cl$_2$ (**8**)
CCDC No	2001557	2001558
Empirical formula	$C_{23}H_{29}Cl_2FeN_5O_4S_2$	$C_{23}H_{29}Cl_2FeN_5O_4S_2$
Formula weight	630.38	630.38
Temperature/K	173.00(10)	173.00(10)
Crystal system	monoclinic	monoclinic
Space group	*I*2/*a*	$P2_1/m$
a/Å	20.82730(10)	7.80925(5)
b/Å	13.99670(10)	18.68619(9)
c/Å	19.10800(10)	9.50696(5)
α/°	90	90
β/°	95.4270(10)	93.6941(5)
γ/°	90	90
Volume/Å^3	5545.27(6)	1384.422(13)
Z	8	2
ρ_{calc}g/cm^3	1.510	1.512
μ/mm^{-1}	7.875	7.886
F(000)	2608.0	652.0
Crystal size/mm^3	0.15 × 0.075 × 0.025	0.321 × 0.141 × 0.03
Radiation	CuKα (λ = 1.54184)	CuKα (λ = 1.54184)
2Θ range for data collection/°	7.62 to 154.35	9.322 to 154.378
Index ranges	$-26 \le h \le 26, -17 \le k \le 16, -24 \le l \le 21$	$-8 \le h \le 9, -17 \le k \le 23, -11 \le l \le 12$
Reflections collected	21839	15141
Independent reflections	5651 [R_{int}= 0.0383, R_{sigma}= 0.0290]	2995 [R_{int}= 0.0241, R_{sigma}= 0.0166]
Data/restraints/parameters	5651/0/340	2995/0/178
Goodness-of-fit on F^2	1.091	1.047
Final R indexes [I>=2σ (I)]	$R_1 = 0.0323$, $wR_2 = 0.0891$	$R_1 = 0.0334$, $wR_2 = 0.0890$
Final R indexes [all data]	$R_1 = 0.0351$, $wR_2 = 0.0909$	$R_1 = 0.0341$, $wR_2 = 0.0896$
Largest diff. peak/hole / e Å^{-3}	0.39/-0.37	0.78/-0.73

Table S4. Bond lengths for **2**.

Atom	Length/Å	Atom	Length/Å
Fe1–Cl1	2.2961(6)	N3–C10	1.354(2)
Fe1–Cl2’	2.6662(5)	N3–C12	1.476(2)
Fe1–Cl2	2.3464(5)	C1–C2	1.382(3)
Fe1–N1	2.1142(16)	C2–C3	1.382(3)
Fe1–N2	2.1639(15)	C3–C4	1.379(3)
O1–C6	1.229(2)	C4–C5	1.385(3)
N1–C1	1.341(2)	C5–C6	1.511(3)
N1–C5	1.350(2)	C7–C8	1.418(3)
N2–C6	1.361(2)	C7–C11	1.411(3)
N2–C7	1.378(2)	C8–C9	1.362(3)
N3–C9	1.346(3)	C10–C11	1.365(3)

’ 1-x,1-y,1-z

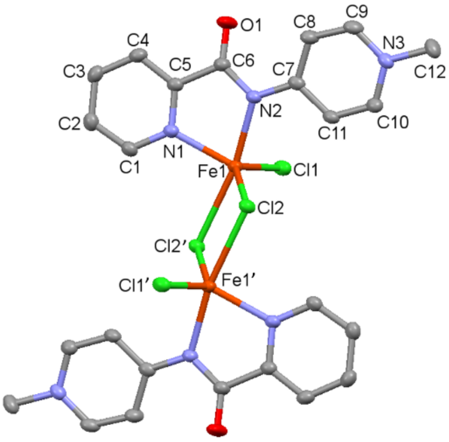

To calculate the C–C bond alteration between C_α–C_β and C_β–C_γ the following formula was used:
Δd = (C7–C8 + C7–C11)/2 – (C8–C9 + C10–C11)/2
(1.418 + 1.411)/2 – (1.362 + 1.365)/2 = 0.051 Å

Table S5. Bond lengths for **3**.

Atom	Length/Å	Atom	Length/Å
Fe1–Cl1	2.3914(8)	C2–C3	1.358(6)
Fe1–O1	2.0927(18)	C3–C4	1.391(5)
Fe1–N1	2.189(2)	C4–C5	1.385(4)
Fe1–N4	2.278(2)	C5–C6	1.504(4)
Fe1–N5	2.195(2)	C7–C8	1.400(4)
Fe1–N6	2.240(2)	C7–C11	1.405(4)
O1–C6	1.272(3)	C8–C9	1.355(4)
N1–C1	1.341(4)	C10–C11	1.354(4)
N1–C5	1.344(4)	C13–C14	1.387(4)
N2–C6	1.308(3)	C14–C15	1.354(5)
N2–C7	1.377(4)	C15–C16	1.356(5)
N3–C9	1.348(4)	C16–C17	1.381(5)
N3–C10	1.344(3)	C18–C19	1.380(4)
N3–C12	1.474(4)	C19–C20	1.369(4)
N4–C13	1.329(4)	C20–C21	1.360(4)
N4–C17	1.320(4)	C21–C22	1.386(4)
N5–C18	1.331(4)	C23–C24	1.386(4)
N5–C22	1.331(3)	C24–C25	1.380(4)
N6–C23	1.347(4)	C25–C26	1.362(4)
N6–C27	1.338(3)	C26–C27	1.377(4)
C1–C2	1.372(5)		

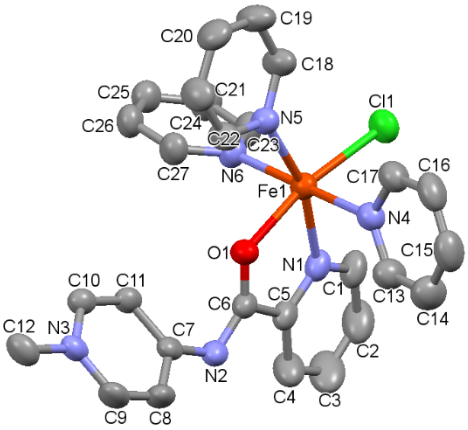

To calculate the C–C bond alteration between C_α–C_β and C_β–C_γ the following formula was used:
Δd = (C7–C8 + C7–C11)/2 – (C8–C9 + C10–C11)/2
(1.400 + 1.405)/2 – (1.355 + 1.354)/2 = 0.048 Å

Table S6. Bond lengths for **6**.

Atom	Length/Å	Atom	Length/Å
Fe1–Cl2	2.3377(5)	N23–C21	1.357(2)
Fe1–Cl3	2.3205(5)	N36–C35	1.352(2)
Fe1–N20	2.2476(14)	N36–C31	1.341(3)
Fe1–N12	2.0696(14)	N36–C37	1.476(2)
Fe1–N23	2.2559(14)	O22–C21	1.233(2)
O19–C18	1.231(2)	C33–C34	1.414(2)
N20–C33	1.370(2)	C33–C32	1.419(2)
N20–C18	1.363(2)	C13–C18	1.508(2)
N12–C13	1.338(2)	C13–C14	1.387(2)
N12–C17	1.339(2)	C26–C27	1.420(2)
N29–C28	1.348(3)	C26–C25	1.412(2)
N29–C30	1.469(2)	C34–C35	1.366(2)
N29–C24	1.357(2)	C32–C31	1.367(3)
N23–C26	1.374(2)	C17–C21	1.511(2)
		C17–C16	1.385(2)
		C14–C15	1.385(3)
		C27–C28	1.365(3)
		C16–C15	1.390(3)
		C24–C25	1.360(3)

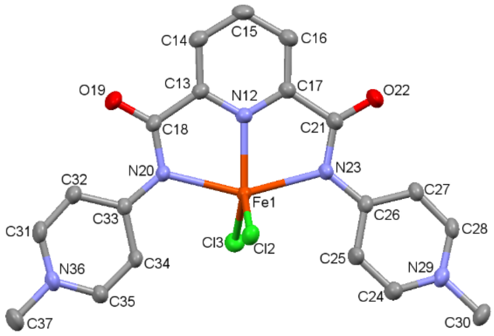

To calculate the C–C bond alteration between C_α–C_β and C_β–C_γ the following formula was used:
Δd = (C25–C26 + C26–C27 + C32–C33 + C33–C34)/4 – (C24–C25 + C27–C28 + C31–C32 + C34–C35)/4 = 0.052 Å

Table S7. Bond lengths for **8**.

Atom	Length/Å	Atom	Length/Å
Fe1–Cl1	2.3563(7)	N2–C7	1.329(2)
Fe1–Cl2	2.2759(8)	N3–C8	1.3387(19)
Fe1–O1	2.1797(12)	C1–C2	1.412(2)
Fe1–N3	2.109(2)	C2–C3	1.376(3)
O1–C7	1.259(2)	C3–C4	1.392(3)
N1–C1	1.373(2)	C4–C5	1.361(3)
N1–C5	1.359(2)	C7–C8	1.504(2)
N1–C6	1.478(2)	C8–C9	1.391(2)
N2–C1	1.353(2)	C9–C10	1.391(2)

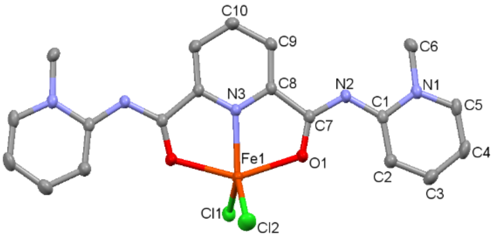

To calculate the C–C bond alteration the following formula was used:
Δd = (C1-C2 + C3-C4)/2 – (C2-C3 + C4-C5)/2
(1.412 + 1.392)/2 – (1.376 + 1.361)/2 = 0.034 Å

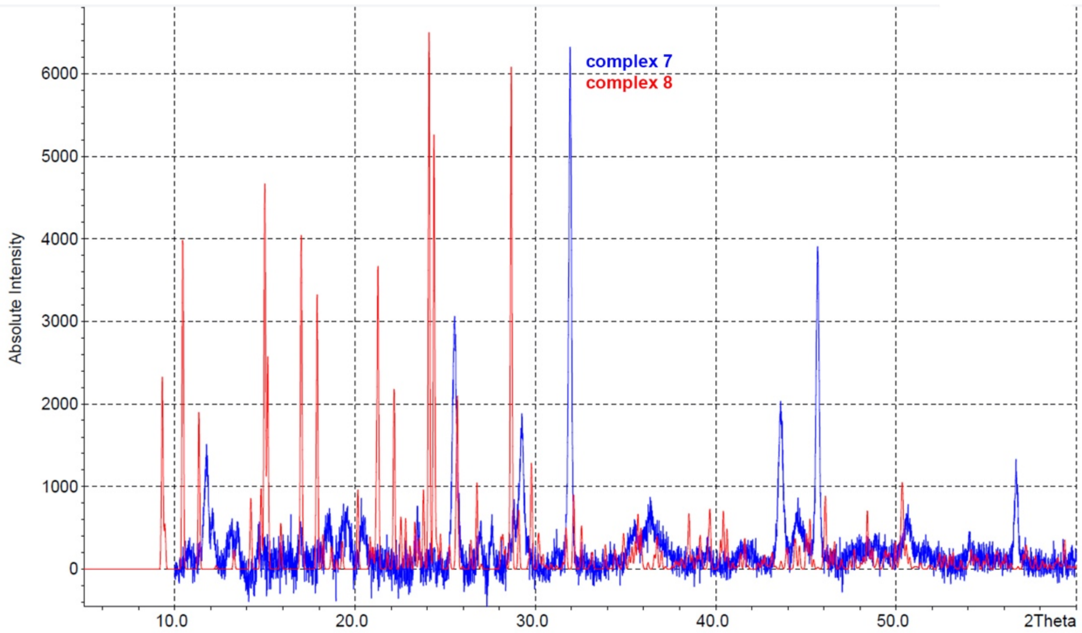

Figure S19. Comparison of calculated powder diffraction pattern for complex **8** (red) and measured data of complex **7** (blue).

6. References

S1. Oxford Diffraction, 2018. *CrysAlisPro*, Version 1.171.40.39a. Oxford Diffraction Ltd., Yarnton, Oxfordshire, UK.

S2. P. Macchi, H. B. Bürgi, A. S. Chimpri, J. Hauser and Z. Gal, Low-energy contamination of Mo microsource X-ray radiation: analysis and solution of the problem, *J. Appl. Cryst*, 2011, **44**, 763–771.

S3. G. M. Sheldrick, SHELXT - Integrated space-group and crystal-structure determination, *Acta Cryst*. 2015, **A71**, 3–8.

S4. G. M. Sheldrick, Crystal structure refinement with SHELXL, *Acta Cryst*. 2015, **C71**, 3–8.

S5. O. V. Dolomanov, L. J. Bourhis, R. J. Gildea, J. A. K. Howard and H. Puschmann, *J. Appl. Cryst.*, 2009, **42**, 339–341.